LB-UNet: A Lightweight Boundary-assisted UNet for Skin Lesion Segmentation

Jiahao Xu[1] and Lyuyang Tong[1,2,3,4]✉

[1] School of Computer Science, Wuhan University, Wuhan, China
{Lyuyangtong}@whu.edu.cn
[2] National Engineering Research Center for Multimedia Software, Wuhan University
[3] Institute of Artificial Intelligence, School of Computer Science, Wuhan University
[4] Hubei Key Laboratory of Multimedia and Network Communication Engineering, Wuhan University

Abstract. Skin lesion segmentation is vital in computer-aided diagnosis and treatment of skin diseases. UNet and its variants have been widely utilized for skin lesion segmentation. However, resource constraints limit the deployment of larger parameter models on edge devices. To address this issue, we propose a novel lightweight boundary-assisted UNet (**LB-UNet**) for skin lesion segmentation. LB-UNet incorporates the Group Shuffle Attention module (GSA) to significantly reduce the model's parameters and computational demands. Furthermore, to enhance the model's segmentation capability, especially in handling ambiguous boundary, LB-UNet introduces the Prediction Map Auxiliary module (PMA). Briefly, PMA consists of three modules: (1) Segmentation Region and Boundary Prediction module is utilized to predict the segmentation region and boundary of the decoder features; (2) GA-Based Boundary Generator is employed to generate the ground truth boundary map through genetic algorithm; (3) Prediction Information Fusion module enhances the skip connection by leveraging the prediction information. By combining this modules, the region and boundary information is effectively integrated into the backbone. The experiment results on the ISIC2017 and ISIC2018 datasets demonstrate that LB-UNet outperforms current lightweight methods. To the best of our knowledge, LB-UNet the first model with a parameters count limited to **38KB** and Giga-Operations Per Second (GFLOPs) limited to **0.1**. The codes and trained models are publicly available at https://github.com/xuxuxuxuxuxjh/LB-UNet.

Keywords: Skin lesion segmentation · Lightweight · Boundary-assisted.

1 Introduction

In the past decades, skin cancer and its associated expenses have become a major public health issue [18]. According to recent data, melanomas represent approximately 1% of skin cancer cases but are responsible for the majority of skin cancer-related deaths [16]. The biggest challenge in skin cancer diagnosis is the lack of specialized doctors. To address this issue, an effective solution is

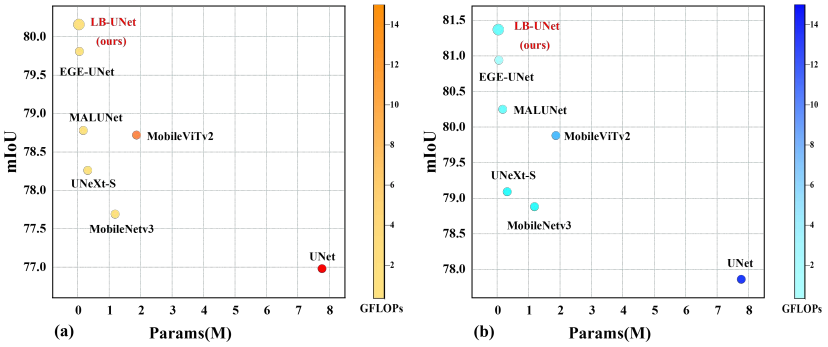

Fig. 1: (a) and (b) respectively show the visualization of comparison results on the ISIC2017 and ISIC2018 dataset. X-axis represents parameter count, Y-axis represents mIoU, and the color depth indicates GFLOPs.

the use of artificial intelligence (AI) for medicine. Deploying lightweight models on smartphones can enable real-time diagnosis like the DermAssist [13] and Skinive [23] apps. Transmitting skin images to remote servers for processing is not allowed to protect patient privacy [18]. Therefore, lightweight models are needed, and transformer-based large models like [2,3,27] may no longer be suitable. Lightweight skin lesion segmentation has gained significant attention in recent years as a crucial and challenging component of automated skin lesion analysis workflows [18]. Valanarasu et al. [25] proposed the UNeXt model, which utilizes tokenized MLP blocks instead of regular convolutional layers, reducing parameters and computational complexity. MALUNet [21] and its extended version EGE-UNet [22] introduce novel attention modules and skip connections, showcasing powerful segmentation performance. However, there is room for improvement in terms of model parameters and segmentation accuracy, particularly in addressing the ambiguity of structure boundary in skin lesion segmentation.

In this paper, we propose a novel boundary-assisted lightweight skin lesion segmentation model called LB-UNet. It not only achieves a significant reduction in model parameters but also demonstrates excellent performance in addressing ambiguous boundary in skin lesion segmentation. Specifically, LB-UNet introduces two key modules: Group Shuffle Attention modules (GSA) and Predictive Map Auxiliary modules (PMA). On one hand, inspired by EGE-UNet [22] and ShuffleNet [29], we propose GSA to reduce parameters. It divides the input into different groups and utilizes Hadamard Product Attention within each group. However, unlike EGE-UNet [22], we do not change the axes of attention but utilize Group Shuffle operation to more effectively capture information. On the other hand, we introduce PMA to enhance the model's ability to segment ambiguous boundary. PMA consists of three sub-modules: Segmentation Region and Boundary Prediction module (RBP), Prediction Information Fusion module (PIF), and GA-Based Boundary Generator (GBG). LB-UNet enhances its learning of crucial region and boundary information by comparing the predictive

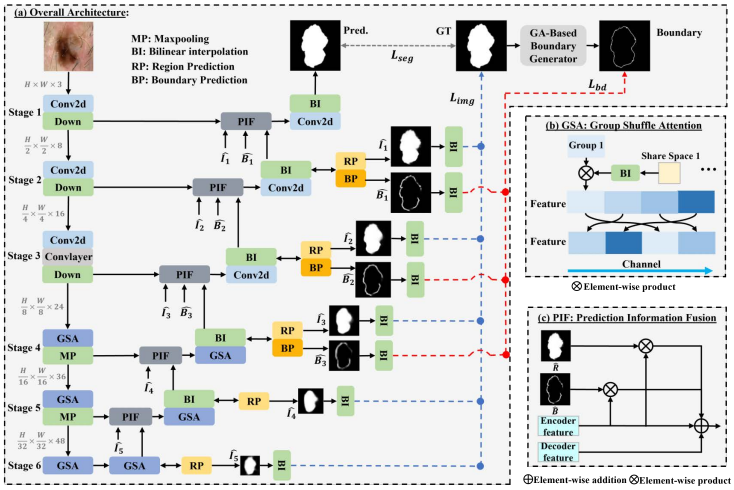

Fig. 2: (a) The overview of LB-UNet; (b) The architecture of Group Shuffle Attention module; (c) The architecture of Prediction Information Fusion module.

maps generated by RBP with both the ground truth and the boundary maps generated by GBG. RBP effectively integrates deep supervision into the segmentation model like [5,8] . In contrast to [5], which utilizes deconvolution to match the label size, we create feature maps through 1×1 convolutions and resize them to match the label size using bilinear interpolation. AD Diagnostics [8] uses deep supervision in upper layers for fine-tuning the model, while we employ deep supervision in intermediate layers to enhance boundary perception. PIF combines predictive maps with skip connections, focusing on essential region and boundary. Inspired by previous research, we improved Lee's [11] boundary key point selection algorithm and proposed GBG. GBG employs a genetic algorithm instead of random selection to generate high-quality boundary key point in fewer iterations. Compared to the method that BAT [28] uses, which employs circles with a radius of 10 to calculate the lesion area, GBG is capable of adapting to images of different sizes.

In summary, our contributions can be divided into two aspects: (1) We propose GSA and PMA, where GSA effectively reduces parameters, while PMA enhances the model's segmentation capability. (2) We introduce LB-UNet, a lightweight skin lesion segmentation model that is the first model with parameters count below 38KB and GFLOPs below 0.1.

2 LB-UNet

2.1 Architecture Overview:

The architecture of our proposed LB-UNet is illustrated in Fig.2(a). LB-UNet is a UNet-based model composed of an encoder, decoder and PMA. The encoder

and decoder consist of six stages, with channel sizes of {8, 16, 24, 32, 48, 64}. The first three stages employ regular convolutional layers with a kernel size of 3, while the last three stages utilize GSA, which offers reduced parameters count and computational demands. For downsampling in the encoder, we replace the max-pooling operation with a 2×2 convolutional operation. Additionally, after the convolutional operation in the encoder of Stage 3, we incorporate the ConvLayer, which has demonstrated excellent performance in ConvUNeXt [7]. PMA integrates well with the UNet framework, performing segmentation region prediction in Stages 2-6 and boundary prediction in Stages 2-4. Unlike the simple skip connections in UNet, LB-UNet adopts prediction-based skip connections and utilizes PIF to focus on the segmentation region and boundary information.

2.2 Group Shuffle Attention module:

Due to the high parameters of the convolutional layer in deep networks, we introduce the GSA to replace it, as shown in Fig. 2(b). First, we divide the input into four groups based on channels, and each group is processed separately, effectively reducing the parameters. Then, for each group, we employ linear complexity HPA [22] to construct an 8×8 shared memories [6] for information retrieval. Finally, we apply shuffle operation to adjust the order of groups and merge them along the channel dimension, followed by utilizing depth-wise separable convolution [10] to fuse the information.

2.3 Predictive Map Auxiliary module:

To improve the boundary segmentation capability, we propose PMA. PMA consists of three parts: RBP, PIF and GBG.

Segmentation Region and Boundary Prediction module: We propose RBP, which utilizes two separate convolutional modules. One module is dedicated to predicting the segmentation region, while the other module focuses on predicting the boundary. To preserve this prediction information, we further employ a residual attention scheme [26]. The above process can be expressed by formulas (1) to (2).

$$\hat{R}^i = \delta(c_{1\times1}(F^i)) \quad , \quad \hat{B}^i = \delta(c_{1\times1}(F^i)) \tag{1}$$

$$\begin{cases} D^i = F^i + F^i \times \hat{R}^i + F^i \times \hat{B}^i & (i = 2, 3, 4) \\ D^i = F^i + F^i \times \hat{R}^i & (i = 5, 6) \end{cases} \tag{2}$$

where $F^i \in \mathbb{R}^{w^i \times h^i \times c^i}$ represents the feature of i-th decoder layer, $\hat{R}^i \in \mathbb{R}^{w^i \times h^i \times 1}$ represents the predictive region feature, $\hat{B}^i \in \mathbb{R}^{w^i \times h^i \times 1}$ represents the predictive boundary feature, $D^i \in \mathbb{R}^{w^i \times h^i \times c^i}$ represents the preserved feature, δ is a sigmoid function, and $c_{1\times1}$ denotes convolution function with kernel size of 1.

Prediction Information Fusion module: In traditional UNet [20] models, the encoder feature is directly added to the decoder feature through skip connections. Different from previous fusion methods, we design the PIF to specifically focus

Algorithm 1 Genetic Algorithm-Based Boundary key point selection algorithm

Input: number of key points n, population size N_P, initialize iteration count T_1, genetic iteration count T_2, crossover probability β, mutation probability γ
Output: boundary key point set $S_{\max}$ with the maximum fitness.
for i = 1, 2, ..., T_1 **do**
    $P_*^i \leftarrow$ randomly generate a set of n points $\{(x_1, y_1), (x_2, y_2), ..., (x_n, y_n)\}$
end for
Calculate fitness $IOU(R_{GT}, f(P_*^i))$
$P_0 \leftarrow$ select the N_p individuals with the highest $IOU(R_{GT}, f(P_*^i))$.
for t = 1, 2, ..., T_2 **do**
    for i = 1, 2, ..., N_P **do**
        Parent1, Parent2 $\leftarrow$ roulette wheel selection from P_{t-1} based on IOU
        if $rand < \beta$ **then**
            Offspring $\leftarrow$ *crossover*(Parent1, Parent2)
        else
            Offspring $\leftarrow$ Parent1
        end if
        if $rand < \gamma$ **then**
            Offspring $\leftarrow$ *mutation*(Offspring)
        end if
        $P_t^i \leftarrow$ Offspring
    end for
    Calculate fitness $IOU(R_{GT}, f(P_t^i))$
    if $f(P_t^i) > f(S_{\max})$ **then**
        $S_{\max} \leftarrow P_t^i$, where $i = \arg\max\left(IOU(R_{GT}, f(P_t^i))\right)$
    end if
end for
return $S_{\max}$

on the features related to segmentation region and boundary. As shown in Fig. 2(c), the encoder feature related to segmentation region and boundary is added to the preserved decoder feature with specific weights, providing an additional contribution. The PIF module can be expressed as:

$$\begin{cases} V^{i-1} = D^i + E^i + w_1^i \times E^i \times \hat{R}^i + w_2^i \times E^i \times \hat{B}^i & (i = 2, 3, 4) \\ V^{i-1} = D^i + E^i + w_1^i \times E^i \times \hat{R}^i & (i = 5, 6) \end{cases} \tag{3}$$

where E^i represents the feature of i-th encoder layer, the result V^{i-1} is fed into $(i-1)$-th decoder layer. In this paper, we set w_1^i to 0.5, 0.4, 0.3, 0.2, 0.1 for i from 2 to 6, and w_2^i to 0.3, 0.2, 0.1 for i from 2 to 4.

GA-Based Boundary Generator: GBG is a module that generates a specialized ground truth boundary map. The ground truth boundary map consists of boundary line and key point components. The boundary line component can be obtained by conventional edge detection algorithm [1]. For the key point component, we propose a GA-based boundary key point selection algorithm. First, we utilize a previous method [11] for evaluating key point. Let

$S = \{(x_1, y_1), (x_2, y_2), \ldots, (x_n, y_n)\}$ denotes a set of n key points. The function $f(\cdot)$ is defined as connecting the points in set S sequentially to form a boundary region. The evaluation criterion and fitness function are based on the Intersection Over Union (IOU) value between the region $f(S)$ formed by the key points and the ground truth region R_{GT}. Then, we use a genetic algorithm to search for the key point set with the maximum IOU value. We start by randomly generating T_1 sets of key points to form an initial population P_0 of size N_P. Next, we perform T_2 iterations of genetic evolution to update the population. Finally, the key point with the maximum IOU value among all populations is identified as the final answer. Algorithm 1 describes the details of the proposed genetic algorithm-based boundary key point selection algorithm.

2.4 Loss function:

In our study, we adopted the group loss from EGE-UNet [22] and added an additional boundary loss function. This modification enables LB-UNet to not only focus on segmentation regions but also to pay more attention to the finer details of boundary. Our loss function can be expressed as formulas (4) to (7).

$$\mathcal{L}_{Seg} = \mathcal{L}_{BCE}(y, \hat{y}) + 2 \times \mathcal{L}_{DICE}(y, \hat{y}), \tag{4}$$

$$\mathcal{L}^i_{Region} = 0.5 \times \mathcal{L}_{BCE}(y, \mathrm{BI}(\hat{R}^i)) + \mathcal{L}_{DICE}(y, \mathrm{BI}(\hat{R}^i)) \tag{5}$$

$$\mathcal{L}^i_{Boundary} = 0.5 \times \mathcal{L}_{BCE}(\mathrm{GBG}(y), \mathrm{BI}(\hat{B}^i)) + \mathcal{L}_{DICE}(\mathrm{GBG}(y), \mathrm{BI}(\hat{B}^i)) \tag{6}$$

$$\mathcal{L}_{Total} = \mathcal{L}_{Seg} + \sum_{i=2}^{6} \lambda_i \times \mathcal{L}^i_{Region} + \sum_{i=2}^{4} \mu_i \times \mathcal{L}^i_{Boundary} \tag{7}$$

where $\mathcal{L}_{BCE}$ and $\mathcal{L}_{DICE}$ represent binary cross-entropy and dice loss, BI denotes bilinear interpolation, GBG denotes GA-Based Boundary Generator. λ_i is the weight of region feature $\hat{R}^i$ for different stage, and μ_i is the weight of boundary feature $\hat{B}^i$ for different stage. In this paper, we set λ_i to 0.5, 0.4, 0.3, 0.2, 0.1 for i from 2 to 6, and μ_i to 0.3, 0.2, 0.1 for i from 2 to 4.

3 Experiments

Datasets: To effectively evaluate our proposed LB-UNet model, we selected two commonly used skin lesion segmentation datasets, ISIC2017 [12] and ISIC2018 [4,24]. ISIC2017 consists of 2150 dermoscopy images, while ISIC2018 contains 2694 dermoscopy images. Consistent with prior research [21], we randomly split the datasets into training and testing sets at a 7:3 ratio. We normalized all the images and resized them to a size of 256×256. For the training set, we applied image augmentation techniques such as horizontal flipping, vertical flipping, and random rotation to enhance the data.

Implementation Details: LB-UNet is implemented with Pytorch [19] framework. All experiments are performed on a single NVIDIA GeForce RTX 3090

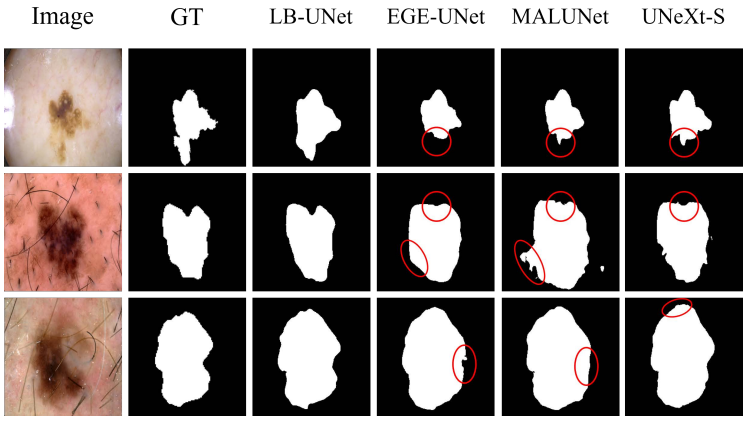

Fig. 3: Visualization of some predictions on the ISIC2018 dataset.

GPU. We utilize AdamW [15] as the optimizer with a learning rate of 0.001 and a weight decay of 0.01. For the scheduler, we select the CosineAnnealingLR [14] with a maximum number of iterations of 50 and a minimum learning rate of 0.00001. The batch size is set to 8, and we train LB-UNet for a total of 300 epochs. To assess our proposed method, we employ Mean Intersection over Union(mIoU) and Dice similarity score(DSC) as evaluation metrics. In addition, Params and GFLOPs are utilized to assess the number of parameters and the computational complexity respectively. To generate the ground truth boundary map, we selected 6 key points as described by Lee [11]. We initialized a population of size 300 with 2000 random iterations, followed by 100 genetic iterations($n = 6, T_1 = 2000, T_2 = 100, N_p = 300$).

Comparative results: We compared the performance of LB-UNet with the state-of-the-art lightweight skin lesion segmentation models on the ISIC2017 and ISIC2018 datasets. The results are presented in Table 1. Please note that our focus is on comparing the models based on segmentation performance, as well as the number of parameters and computational complexity. In comparison to the current state-of-the-art model EGE-UNet [22], our model not only demonstrates superior segmentation performance but also reduces the number of model parameters by 1.4x. Additionally, taking the results on the ISIC2018 dataset as an example, LB-UNet achieves a 2.28% increase in mIoU and a 1.21% increase in DSC compared to UNeXt-S [25], while reducing the model parameters by 11.9%. In Figure 3, we present the visualization of models' segmentation results. This figure visually demonstrates the impressive boundary detail segmentation capabilities of LB-UNet.

Ablation results: To demonstrate the effectiveness of the proposed modules, we conducted ablation experiments on the ISIC2018 dataset. In this paper, we adopted a six-stage U-shaped architecture with symmetric encoder and decoder components, referenced from MALUNet [21], as our baseline model. Each stage's

Table 1: Comparative experimental results on the ISIC2017 and ISIC2018.

Dataset	Model	Params(M)↓	GFLOPs↓	mIoU(%)↑	DSC(%)↑
ISIC2017	UNet [20]	7.77	13.76	76.98	86.99
	MobileViTv2 [17]	1.87	0.70	78.72	88.09
	MobileNetv3 [9]	1.19	0.10	77.69	87.44
	UNeXt-S [25]	0.32	0.10	78.26	87.80
	MALUNet [21]	0.177	0.085	78.78	88.13
	EGE-UNet [22]	0.053	**0.072**	79.81±0.10	88.77±0.06
	LB-UNet(ours)	**0.038**	0.098	**80.13±0.41**	**88.86±0.28**
ISIC2018	UNet [20]	7.77	13.76	77.86	87.55
	MobileViTv2 [17]	1.87	0.70	79.88	88.81
	MobileNetv3 [9]	1.19	0.10	78.55	87.98
	UNeXt-S [25]	0.32	0.10	79.09	88.33
	MALUNet [21]	0.177	0.085	80.25	89.04
	EGE-UNet [22]	0.053	**0.072**	80.94±0.11	89.46±0.07
	LB-UNet(ours)	**0.038**	0.098	**81.37±0.10**	**89.54±0.05**

Table 2: Ablation performances of the single module.

Model	Params(M)↓	GFLOPs↓	mIoU(%)↑	DSC(%)↑
Baseline	0.107	0.072	80.03	88.24
Baseline+GSA	0.028	0.059	80.50	88.36
Baseline+PMA	0.107	0.073	81.07	88.97
Baseline+ConvLayer	0.112	0.097	81.36	89.31
Baseline+Down	0.110	0.087	81.23	88.99

Table 3: Ablation performances of ground truth boundary map.

Model	Boundary line	Genetic KP	Random KP	mIoU(%)↑	DSC(%)↑
LB-UNet	✓	✓		81.37	89.54
	✓		✓	81.29	89.44
		✓		81.20	89.48
			✓	81.18	89.29

encoder and decoder layer consists of a convolution module with a kernel size of 3, and the number of channels in each stage is $\{8, 16, 24, 36, 48, 64\}$. In Table 2, we conducted ablation experiments on each single module. Note that (1) GSA replaces the convolution modules in Stages $4-6$, (2) The ConvLayer, referenced from ConvUNeXt [7], is only utilized in the encoder part of Stage 3. (3) The Down operation replaces the max-pooling layers in Stages $1-3$ with convolution functions of kernel size 2. Table 3 presents the ablation results for the ground truth boundary maps. LB-UNet achieves better segmentation accuracy when using boundary maps with boundary line compared to those without boundary line. Using genetic key point outperforms using random key point. Please note that the random key point mentioned here is generated through random iterations for 40,000 times, while the genetic key point is generated through genetic iterations with a population size of 300 for 100 iterations.

4 Conclusion

In this paper, we propose a lightweight model based on segmentation region and boundary prediction, which can be applied to mobile dermoscopes and edge devices. We introduce two advanced modules. GSA utilizes a linear attention mechanism to significantly reduce the number of parameters and computational complexity. PMA effectively captures information from the segmentation region, particularly the boundary, to enhance the segmentation accuracy. In the PMA module, we propose a novel boundary key point selection algorithm based on genetic algorithm, which produces enhanced results. Looking ahead to future work, our plan is to implement LB-UNet on mobile devices to achieve real-time segmentation detection. Additionally, LB-UNet is proposed only for skin lesion segmentation, and we intend to extend our efficient design to other tasks.

Acknowledgement. This work was supported in part by the National Key Research and Development Program of China under Grants 2023YFC2705700, the National Natural Science Foundation of China under Grants 62306217 and 62225113, the Postdoctoral Fellowship Program of CPSF under Grant Number GZC20231987, the China Postdoctoral Science Foundation under Grant Number 2024T170686 and 2024M752471, the Major Program (JD) of Hubei Province (2023BAA017), the Innovative Research Group Project of Hubei Province under Grants 2024AFA017.

Disclosure of Interests

The authors declare that we have no competing interests.

References

1. Canny, J.: A computational approach to edge detection. IEEE Transactions on pattern analysis and machine intelligence (6), 679–698 (1986)
2. Cao, H., Wang, Y., Chen, J., Jiang, D., Zhang, X., Tian, Q., Wang, M.: Swin-unet: Unet-like pure transformer for medical image segmentation. In: European conference on computer vision. pp. 205–218. Springer (2022)
3. Chen, J., Lu, Y., Yu, Q., Luo, X., Adeli, E., Wang, Y., Lu, L., Yuille, A.L., Zhou, Y.: Transunet: Transformers make strong encoders for medical image segmentation. arXiv preprint arXiv:2102.04306 (2021)
4. Codella, N., Rotemberg, V., Tschandl, P., Celebi, M.E., Dusza, S., Gutman, D., Helba, B., Kalloo, A., Liopyris, K., Marchetti, M., et al.: Skin lesion analysis toward melanoma detection 2018: A challenge hosted by the international skin imaging collaboration (isic). arXiv preprint arXiv:1902.03368 (2019)
5. Dou, Q., Chen, H., Jin, Y., Yu, L., Qin, J., Heng, P.A.: 3d deeply supervised network for automatic liver segmentation from ct volumes. In: Medical Image Computing and Computer-Assisted Intervention–MICCAI 2016: 19th International Conference, Athens, Greece, October 17-21, 2016, Proceedings, Part II 19. pp. 149–157. Springer (2016)

6. Guo, M.H., Liu, Z.N., Mu, T.J., Hu, S.M.: Beyond self-attention: External attention using two linear layers for visual tasks. IEEE Transactions on Pattern Analysis and Machine Intelligence **45**(5), 5436–5447 (2022)
7. Han, Z., Jian, M., Wang, G.G.: Convunext: An efficient convolution neural network for medical image segmentation. Knowledge-Based Systems **253**, 109512 (2022)
8. Hosseini-Asl, E., Gimel'farb, G., El-Baz, A.: Alzheimer's disease diagnostics by a deeply supervised adaptable 3d convolutional network. arXiv preprint arXiv:1607.00556 (2016)
9. Howard, A., Sandler, M., Chu, G., Chen, L.C., Chen, B., Tan, M., Wang, W., Zhu, Y., Pang, R., Vasudevan, V., et al.: Searching for mobilenetv3. In: Proceedings of the IEEE/CVF international conference on computer vision. pp. 1314–1324 (2019)
10. Howard, A.G., Zhu, M., Chen, B., Kalenichenko, D., Wang, W., Weyand, T., Andreetto, M., Adam, H.: Mobilenets: Efficient convolutional neural networks for mobile vision applications. arXiv preprint arXiv:1704.04861 (2017)
11. Lee, H.J., Kim, J.U., Lee, S., Kim, H.G., Ro, Y.M.: Structure boundary preserving segmentation for medical image with ambiguous boundary. In: Proceedings of the IEEE/CVF conference on computer vision and pattern recognition. pp. 4817–4826 (2020)
12. Li, Y., Shen, L.: Skin lesion analysis towards melanoma detection using deep learning network. Sensors **18**(2), 556 (2018)
13. Liu, Y., Jain, A., Eng, C., Way, D.H., Lee, K., Bui, P., Kanada, K., de Oliveira Marinho, G., Gallegos, J., Gabriele, S., et al.: A deep learning system for differential diagnosis of skin diseases. Nature medicine **26**(6), 900–908 (2020)
14. Loshchilov, I., Hutter, F.: Sgdr: Stochastic gradient descent with warm restarts. arXiv preprint arXiv:1608.03983 (2016)
15. Loshchilov, I., Hutter, F.: Decoupled weight decay regularization. arXiv preprint arXiv:1711.05101 (2017)
16. Mangione, C.M., Barry, M.J., Nicholson, W.K., Chelmow, D., Coker, T.R., Davis, E.M., Donahue, K.E., Jaén, C.R., Kubik, M., Li, L., et al.: Screening for skin cancer: Us preventive services task force recommendation statement. Jama **329**(15), 1290–1295 (2023)
17. Mehta, S., Rastegari, M.: Separable self-attention for mobile vision transformers. arXiv preprint arXiv:2206.02680 (2022)
18. Mirikharaji, Z., Abhishek, K., Bissoto, A., Barata, C., Avila, S., Valle, E., Celebi, M.E., Hamarneh, G.: A survey on deep learning for skin lesion segmentation. Medical Image Analysis p. 102863 (2023)
19. Paszke, A., Gross, S., Massa, F., Lerer, A., Bradbury, J., Chanan, G., Killeen, T., Lin, Z., Gimelshein, N., Antiga, L., et al.: Pytorch: An imperative style, high-performance deep learning library. Advances in neural information processing systems **32** (2019)
20. Ronneberger, O., Fischer, P., Brox, T.: U-net: Convolutional networks for biomedical image segmentation. In: Medical Image Computing and Computer-Assisted Intervention–MICCAI 2015: 18th International Conference, Munich, Germany, October 5-9, 2015, Proceedings, Part III 18. pp. 234–241. Springer (2015)
21. Ruan, J., Xiang, S., Xie, M., Liu, T., Fu, Y.: Malunet: A multi-attention and light-weight unet for skin lesion segmentation. In: 2022 IEEE International Conference on Bioinformatics and Biomedicine (BIBM). pp. 1150–1156. IEEE (2022)
22. Ruan, J., Xie, M., Gao, J., Liu, T., Fu, Y.: Ege-unet: an efficient group enhanced unet for skin lesion segmentation. In: International Conference on Medical Image Computing and Computer-Assisted Intervention. pp. 481–490. Springer (2023)

23. Shpudeiko, V., Sokolov, K., Sidaruk, H.: Artificial intelligence in solving dermatological problems. Dermatology Review/Przeglad Dermatologiczny **109**(5), 361–367 (2022)
24. Tschandl, P., Rosendahl, C., Kittler, H.: The ham10000 dataset, a large collection of multi-source dermatoscopic images of common pigmented skin lesions. Scientific data **5**(1), 1–9 (2018)
25. Valanarasu, J.M.J., Patel, V.M.: Unext: Mlp-based rapid medical image segmentation network. In: International Conference on Medical Image Computing and Computer-Assisted Intervention. pp. 23–33. Springer (2022)
26. Wang, F., Jiang, M., Qian, C., Yang, S., Li, C., Zhang, H., Wang, X., Tang, X.: Residual attention network for image classification. In: Proceedings of the IEEE conference on computer vision and pattern recognition. pp. 3156–3164 (2017)
27. Wang, H., Cao, P., Wang, J., Zaiane, O.R.: Uctransnet: rethinking the skip connections in u-net from a channel-wise perspective with transformer. In: Proceedings of the AAAI conference on artificial intelligence. vol. 36, pp. 2441–2449 (2022)
28. Wang, J., Wei, L., Wang, L., Zhou, Q., Zhu, L., Qin, J.: Boundary-aware transformers for skin lesion segmentation. In: Medical Image Computing and Computer Assisted Intervention–MICCAI 2021: 24th International Conference, Strasbourg, France, September 27–October 1, 2021, Proceedings, Part I 24. pp. 206–216. Springer (2021)
29. Zhang, X., Zhou, X., Lin, M., Sun, J.: Shufflenet: An extremely efficient convolutional neural network for mobile devices. In: Proceedings of the IEEE conference on computer vision and pattern recognition. pp. 6848–6856 (2018)